Journal of Colloid and Interface Science 615 (2022) 59–68

Contents lists available at ScienceDirect

Journal of Colloid and Interface Science

journal homepage: www.elsevier.com/locate/jcis

Chemical electrification at solid/liquid/air interface by surface dipole of self-assembled monolayer and harvesting energy of moving water

Changsuk Yun [1], Thanh Duc Dinh [1], Seongpil Hwang *

Department of Advanced Materials Chemistry, Korea University, Sejong 30019, Republic of Korea

GRAPHICAL ABSTRACT

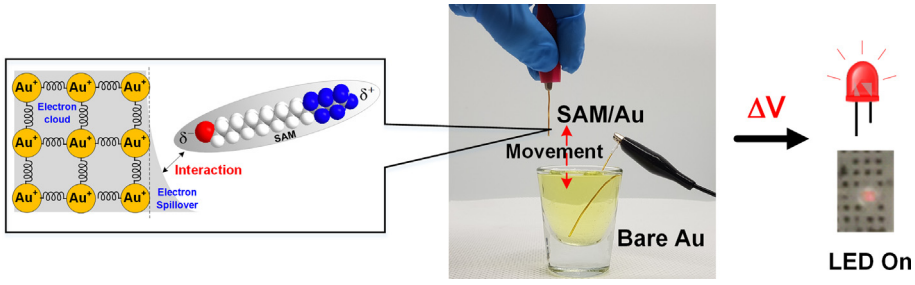

ARTICLE INFO

Article history:
Received 8 September 2021
Revised 10 December 2021
Accepted 17 January 2022
Available online 21 January 2022

Keywords:
Contact electrification
Self-assembled monolayer
Dipole
Energy harvesting
Work function

ABSTRACT

Harvesting energy from water motion is attractive and is considered as a promising component in a microgenerator system for decentralized energy. Recent developments have been shown to rely on spontaneous electrification at the solid-liquid interface, even though the precise mechanism is still under debate. In this paper, we report that the triple-phase boundary of solid/liquid/air can be quantitatively charged by tuning the work function by modifying a self-assembled monolayer (SAM), where a permanent or redox-active dipole controls the polarity and degree of electrification, and by modulating the electrochemical potential of the solution used. With the simple system proposed here, electricity is successfully delivered to turn on a light-emitting diode (LED), demonstrating the potential applicability of the system for energy harvesters.

1. Introduction

The electrode potential is a basic, fundamental and experimentally measurable parameter in electrochemistry, which has also been a key factor related to potentiometry and energy conversion/storage. It is relevant to the extent of excess charge on an electrode surface (σ^M) where minute charges are accumulated/released *via* either charge transfer or the arrangement of ions/dipoles. In terms of thermodynamics, the electrode potential with redox couples in an electrolyte is referred to as Nernstian behavior in an equilibrium state. In electrolysis, an external power source such as potentiostat supplies excess charges to a conductive electrode, followed by the formation of a potential difference across the electrical double layer (EDL), where ions and polar molecules in the electrolyte are redistributed according to the excess charge on the electrode [1]. On the other hand, the redistribution of ions or dipoles on the electrolyte side induces a change in the spillover electrons in the Jellium model, developing electrode potential in a galvanic electrochemical cell [2,3]. The interfacial potential difference across the electrode-electrolyte interface in both cases is the origin of the electrode potential, whose structure has been modeled according to the Gouy-Chapman-Stern model [4]. Therefore,

* Corresponding author.
E-mail address: sphwang@korea.ac.kr (S. Hwang).
[1] Equal contribution.

https://doi.org/10.1016/j.jcis.2022.01.114
0021-9797/

the electrode potential is independent of the contact area between the conducting electrode and the electrolyte in conventional electrochemistry owing to the constant σ^M. There is no previous work, to the best of our knowledge, which reports the dynamic change of the electrode potential by the modulation of the contact area, except for electrokinetic phenomena such as the streaming potential and streaming current from the motion of ions at the EDL [5–7].

Global climate change has initiated research on renewable and alternative energy sources instead of fossil fuels. On the one hand, the centralized energy infrastructure is adopting relatively large-scale power generation devices such as photovoltaic cells and wind power systems. On the other, microgeneration is pursuing independent and decentralized energy through small-scale and renewable supplies. Energy from mechanical motions in everyday life would be a prospective candidate for the latter. Piezoelectricity [8] and triboelectric nanogenerator (TENG) [9] have been investigated in an effort to convert mechanical energy into electricity based on all-solid-state systems, though high stress and the low charge density levels associated with these devices could limit their power. However, a solid-liquid interface may be slippery such that even very weak mechanical motion from a fluid can be converted to other types of energy. These approaches rely on either electrokinetic phenomena or variable capacitors, but the requirement of external voltage remains essential for the initial charging of the interface. Recently, contact electrification at the solid-liquid interface has been exploited to harvest the mechanical energy from natural water in what has been termed blue energy, which ranges from raindrops to the wave energy in rivers and oceans [10]. Carbon-based materials such as carbon nanotube yarn [11] and graphene [12] have been widely investigated in relation to this. Chemically modified surfaces with functional materials have also been employed [13–15]. These findings were well summarized in recent reviews [16–18]. The mechanism of electrification at the solid/liquid interface is significant during the drive to enhance and develop energy harvesting devices. The adsorption of ions [19,20], the tribovoltaic effect followed by a charge transfer at the semiconductor/liquid interface [21,22], and the hybrid two-step model [23] have been introduced. Nonetheless, the mechanism underlying electrification at the solid/liquid interface remains a subject of much debate. From the standpoint of physical electrochemistry, there are several ambiguous points. On the one hand, the adsorption of charged particles such as ions induces the same amount of σ^M (normalized against the area), resulting in the independence of the electrode potential in the contact area. Furthermore, the driving force of ion adsorption (chemisorption) onto an inert passivation layer such as Teflon or SiO_2 was not thoroughly explained in the aforementioned studies [13,24]. On the other hand, the electrochemical potential of the solution phase (corresponding to the Fermi level) is not well defined because the solutions in most of previous works consisted of distilled water or simple electrolytes without redox couples. Therefore, the origin of electrification in a waving or mechanical energy harvester from a solid-liquid system is still ambiguous and methods to control electrification are considered to be at the early stage of trial and error, to the best of our knowledge.

Herein, we envisioned an extremely simple model system to investigate the mechanism of the electrode potential as modulated by the contact area at the triple-phase solid/liquid/air interface, as shown in Scheme 1. Gold was selected as the electrode material due to its inertness, good conductivity, and the well-established surface chemistry. In order to control the immersion depth into the electrolyte, the gold electrode was mounted to a micropositioner and finely translated along the z-axis. A self-assembled monolayer (SAM) was adopted as a surface modifier or as a functional coating to tune the hydrophobicity of the electrode, the adsorption of the ions, the charge transfer across the interface, and the change in the work function of Au ($\bar{\mu}_{e,Au}$), whose structure and properties at the interface have been extensively investigated [25–27]. On the liquid side as opposed to the solid part, the electrochemical potential of the electrolyte ($\bar{\mu}_{solution}$) was adjusted by changing the ratio of the redox couple of $Fe(CN)_6^{3-}/Fe(CN)_6^{4-}$. The electrode potential would be independent of the contact area from classical electrochemistry, *vide supra*, to the best of our knowledge. Surprisingly, this simple model can elucidate the variation of the electrode potential with the contact area at the triple-phase boundary. The polarity and degree of electrification at the interface were successfully tuned by the difference between $\bar{\mu}_{solution}$ and $\bar{\mu}_{e,Au}$. Afterwards, $\bar{\mu}_{e,Au}$ was engineered by the surface potential (χ) from the dipole of the SAM. Our results indicate that χ is the key to the electrification at the solid/liquid/air interface in contrast to the previously suggested EDL model with ion adsorption [6]. In addition, this simple electrochemical system can be utilized for the energy conversion of mechanical motion to electrical energy, inspiring future applications of our findings to energy harvestings or sensors based on the waves of water.

2. Materials and methods

2.1. Materials and chemicals

The self-assembled monolayers (SAMs) were formed on the thermally evaporated Au wafer (200 nm of Au with 4 nm of Ti as an adhesion layer on a Si wafer) and Au wire (Alfa Aesar, 1 mm in diameter) by using 1-octadecanethiol (ODT, purity ≥ 98%), 11-(ferrocenyl)undecanethiol (Fc, purity ≥ 95%), and 1H,1H,2H,2H-perfluoro-1-decanethiol (CF_3, purity ≥ 96%). Potassium ferricyanide ($K_3Fe(CN)_6$, $Fe(CN)_6^{3-}$, purity ≥ 99%) and potassium ferrocyanide ($K_4Fe(CN)_6$, $Fe(CN)_6^{4-}$, purity ≥ 99.95%) were used as the redox species. Potassium chloride (KCl, purity ≥ 99%), potassium nitrate (KNO_3, purity ≥ 99%), and potassium hexafluorophosphate (KPF_6, purity ≥ 99%) were used as the supporting electrolytes, which have different extents of hydrophilicity. All of materials were purchased from Sigma-Aldrich except for the gold electrodes.

2.2. Preparation of the SAMs on the Au electrodes

The Au electrodes were treated in a piranha solution (3:1 (v/v), H_2SO_4:H_2O_2) for 5 min. Subsequently, the clean Au electrodes were immersed in 1 mM ethanolic solutions of SAMs for 15 h. Specifically, the ODT and CF_3 solutions were kept at 33℃ during the whole formation time due to their high melting points while the Fc solution was covered by an Al foil to avoid the exposure to light. The as-prepared SAM/electrodes were washed with absolute ethanol and deionized water (resistivity ≥ 18.2 MΩ·cm) to remove adsorbates from the surface. Finally, the SAM/Au electrodes were dried by N_2 blowing.

2.3. Characterizations

A micropositioner stage (PI, Pollux Box) was used to control the position of the mounted SAM-modified Au electrodes. In the configuration of our proposed model, the SAM/Au and Ag/AgCl (Sat'd KCl) as working and counter-reference electrodes were respectively connected to a positive clip (+) and a negative clip (−) of a Data Acquisition system (NI, DAQ, USB-6002) or Potentiostat (CHI 900B). These two electrodes were immersed in 1 mM $Fe(CN)_6^{3-}$ and/or $Fe(CN)_6^{4-}$ solutions with 0.1 M KCl electrolyte. The electrolytes containing 1 mM $Fe(CN)_6^{4-}$ with 0.1 M K^+X^-(X^-: PF_6^-, NO_3^-, and Cl^-) were adopted to tune the energy level of the Fc/Au

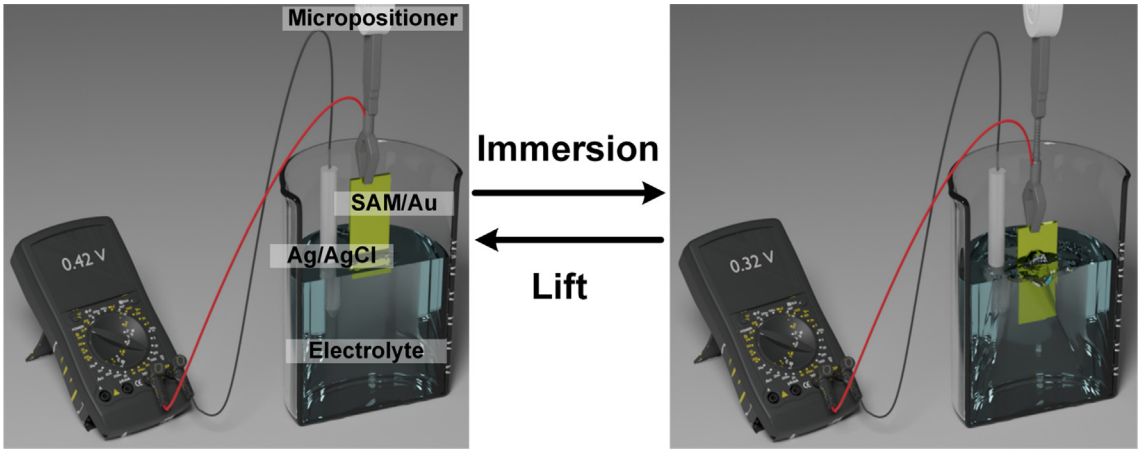

Scheme 1. Illustration of the experimental setup to measure the change in the electrode potential by water movements at the triple-phase interface of solid/liquid/air. The electrode potential *vs.* the Ag/AgCl reference electrode was measured while the immersion depth of the SAM/Au electrode was controlled by a micropositioner.

electrode according to the anions species. During the operation, the working electrode was translated along the z-axis while the Ag/AgCl electrode was fixed, a voltage was generated, based on the change in the contact area between the electrode and the electrolyte.

2.4. Energy harvester for LED

A hybrid cell, which consists of a red light-emitting diode (LED), an electrochemical cell, and a DAQ in serial connection, was adopted. Here, a Ni-MH battery (1.2 V) was added to control the offset potential. The electrochemical cell was composed of 1 mM $Fe(CN)_6^{3-}$ (0.1 M KCl) electrolyte, SAM/Au wire (+), and bare Au wire (−). The SAM/Au electrodes were repeatedly immersed and lifted in/from the solutions manually, while the counter electrode was fixed. The on–off tendency of a LED, which was induced by moving the SAM/electrodes, was demonstrated to be dependent on the kind of SAM. The lighting was recorded via a camera (see Movie S1-S2 in Supplementary Material).

3. Results and discussion

The electrode potential of bare Au in the electrolyte is in good agreement with the predicted value from the Nernst equation and remained nearly constant during the lift/immersion steps of the electrode, as shown in Fig. 1A (black line), indicating the independence of the potential in the contact area at the triple-phase boundary. It should be noted that Au is relatively hydrophilic (Fig. 1B) such that the contact area is not proportional to the displacement of the electrode on the z-axis. The ODT SAM on Au, however, dramatically changes the physicochemical properties of the interface [28]. The electrode potential of ODT/Au itself is very close to the Nernst potential despite the fact that the well-ordered ODT SAM prohibits the charge-transfer process (Figs. S1-S2, Supplementary Information). After the potential reached a steady value, the ODT/Au was repeatedly lifted and immersed with a ten-second interval in each case along the z-axis using a micropositioner (speed of 13 mm/s and total displacement of 5 mm). The red line in Fig. 1A represents the electrode potential during the periodic motion. Lifting the electrode from the solution increases the potential by ca. 105.4 mV from the steady potential of 0.36 V (*vs.* Ag/AgCl), while immersion (returning the electrode to the original position) changes the potential toward the negative direction. In the ODT/Au case, the low surface energy governs the hydrophobicity of the electrode, minimizing the contact line, as observed in Fig. 1C, making the contact area well defined during the translation. Also, it should be noted that the offset in the electrode potential decays exponentially with a time constant (τ) of ca. 4.51 s after mechanical perturbation. The charge-transfer resistance (R_{ct}) and the capacitance of ODT/Au (C_{dl}) were previously reported to be 800 kΩ and 316 nF, respectively [29]. Assuming that the decay in the potential is caused by the charge transfer across the EDL to the redox couple, τ (R_{ct}•C_{dl}) is found to be ca. 0.25 s, which is much smaller than the observed value. This implies that the accumulated/deficient charges on the electrode are redistributed not by the redox reaction but by another slower process. If the redox reaction is a dominant process, transmission of the generated voltage to the external circuit scarcely occurs due to the rapid extinction of the electrode potential. Fortunately, the excess charge on ODT/Au has sufficient time to be delivered to an external circuit.

In order to measure the transmission of electrical energy, a resistor formed a connection between the ODT/Au, bare Au and the electrolyte, as shown in Fig. 2A. The potential difference across the resistor was measured as an indicator of the consumed energy delivered from the ODT/Au electrode. Fig. 2B shows the voltage across the 20 kΩ resistor upon the lift/immersion motion identical to that shown in Fig. 1A. Voltage of ca. 15.1 mV was observed during 1.67 s of the electrode movement, resulting in 11.4 nW ($P = V^2/R$) under this condition. When the electrode is stationary, the voltage is zero due to the null system. The generated energy should be a function of the degree of mechanical motion. In Fig. 2B, dependence of the voltage across the resistor on the translation speed along the z-axis is observed. For lifting motion, the moving durations for a total displacement of 5 mm are 0.38 s, 0.56 s, 1 s, and 1.67 s, corresponding to moving speeds of 13 mm/s, 9 mm/s, 5 mm/s, and 3 mm/s. The voltage values across a 20 kΩ resistor increase linearly with the speeds; these are 4.78 mV, 8.22 mV, 14.0 mV, and 20.8 mV corresponding to the speeds listed above. We experimentally conclude that (1) mechanical energy induces an offset in the electrode potential in the open-circuit condition (Fig. 1A), (2) this energy is successfully transferred to an external resistor (Fig. 2B), and (3) the voltage increases linearly with the speed. There is a still a veiled mechanism, however, which remains unknown. Two models have been suggested thus far: the charge-transfer model and the ion-transfer model [30]. The former requires rapid charge transfer across the interface, but it is not feasible through the well-ordered ODT SAM. The latter is also not plausible because both the low surface energy and the methyl terminal group of ODT would hinder the interaction with the ion spe-

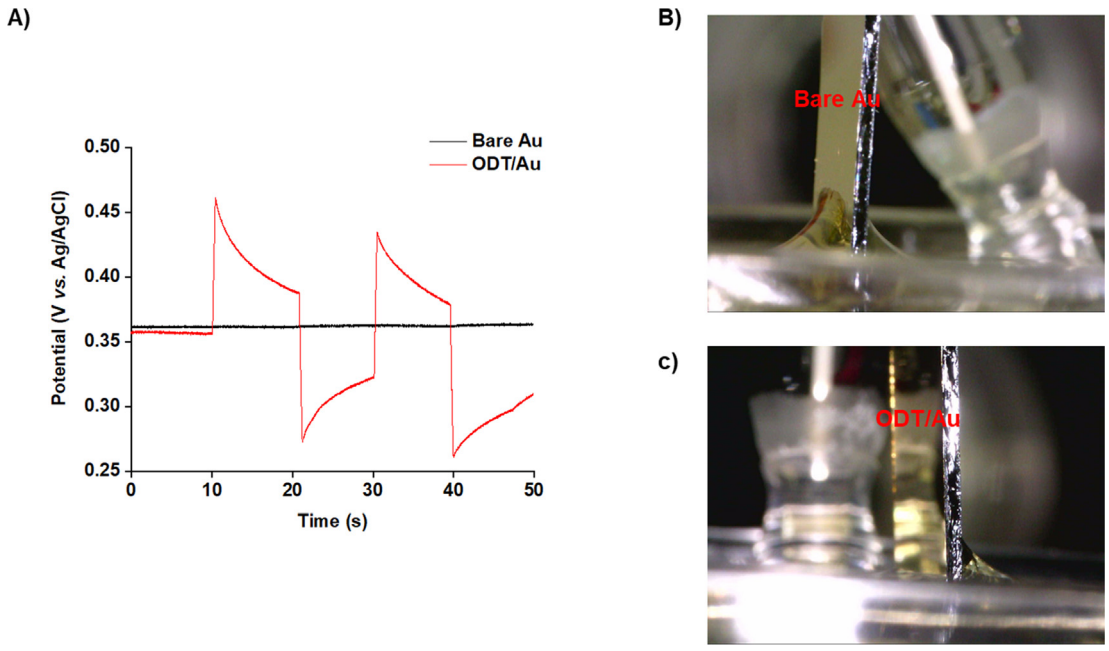

Fig. 1. Measurements of electrode potentials depending on the contact area between the electrode and the electrolyte. (A) Potential responses to variation of the contact area by a micropositioner. Electrolyte: 1 mM $Fe(CN)_6^{3-}$ with 0.1 M KCl. The moving speed is 13 mm/s and the displacement is 5000 μm. Photos of the triple-phase boundary with (B) bare Au and (C) ODT/Au.

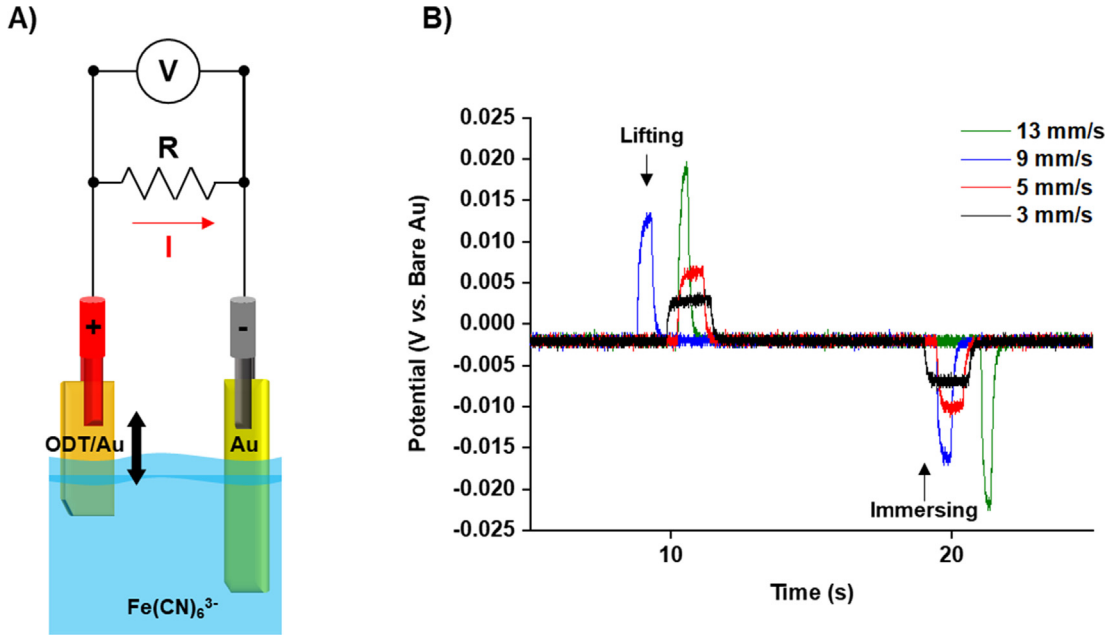

Fig. 2. Measurements of the transmission of the electrical energy to an external 20 kΩ resistor. (A) Illustration of the experimental setup composed of the ODT/Au, bare Au wire and aqueous electrolyte of 1 mM $Fe(CN)_6^{3-}$ with 0.1 M KCl. (B) The dependence of the voltage across a resistor on the moving speeds with the total displacement of 5000 μm in the z-axis.

cies. What drives the electrification at the triple-phase boundary and how can one control the degree of this electrification?

Here, we consider the potential profile across the interface to answer the question above about the charging mechanism, as shown in Scheme 2. For the electrolyte, $\bar{\mu}_{solution}$ is adjusted by altering the chemical composition of the redox species (Scheme 2B). On the other hand, the electrode potential or the electrochemical potential of the electrons ($\bar{\mu}_{e,Au}$) in the conducting phase (i.e. the work function) represents the potential energy of the electrons (Scheme 2A), strongly depending on the dipole of the organized SAM [31,32]. We hypothesize that the potential difference between $\bar{\mu}_{e,Au}$ and $\bar{\mu}_{solution}$ (Scheme 2C) electrifies the charges across the SAM in a steady state, as shown in Scheme 2D. It is important to note that the suggested mechanisms, including the ion adsorption [19,20] and the tribovoltaic effect at the semiconductor-liquid interface [21], are not plausible due to the SAM and conducting Au in our simple model system. Metal with a higher $\bar{\mu}_{e,Au}$ value would be charged positively, while the opposite is true for lower

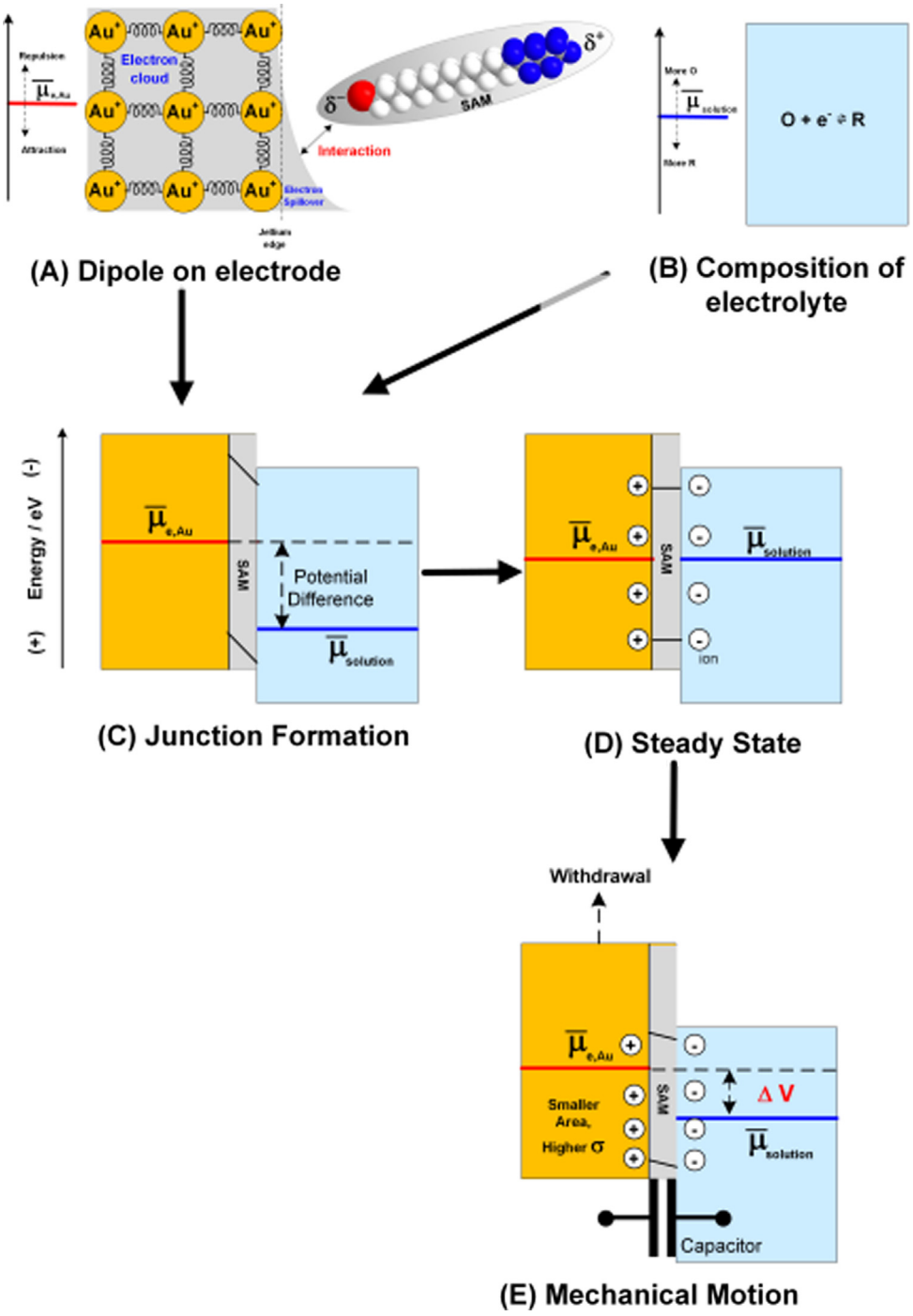

Scheme 2. Illustration of the operation mechanism based on potential profile. (A) Electrochemical potential of a SAM/Au, (B) Electrochemical potential of the electrolyte depending on the composition of the redox couples. (C) Formation of the junction between the SAM/Au and the electrolyte and (D) Charging of an Au electrode in a steady state. (E) Change of the charge density upon the smaller contact area induced by the mechanical motion.

values of $\bar{\mu}_{e,Au}$. The slow charge transfer across the EDL keeps the total charge conserved during the variation of the contact area, making the charge density across the SAM similar to that of a variable capacitor (Scheme 2E). SAM offers (1) low surface energy for a hydrophobic surface, (2) a barrier to prevent rapid charge transfers for thermodynamic equilibrium, (3) a dipole to change $\bar{\mu}_{e,Au}$ and (4) dielectric materials for the capacitor. A strict model of the capacitor was built based on the serial connection between the capacitance of the SAM and that of the EDL. The latter, however, is negligible due to the relatively large value [29,33]. To prove this hypothesis, the work function of the metal was adjusted by the formation of a SAM with an opposite dipole. The Jellium model describes the conducting phase as a lattice of cations with a free electron, where the electron can spill over the metal surface. The degree of these spillover electrons is closely related to the surface charge (σ^M) and work function in a vacuum. Adsorbed polar molecules such as thiols interact strongly with these spillover electrons resulting in a change of $\bar{\mu}_{e,Au}$. Sulfur tails of ODT are partially negative, which results in a decrease in the work function by 1.2 eV from that of bare Au (~5.1 eV) [27]. In contrast, the sulfur tails of

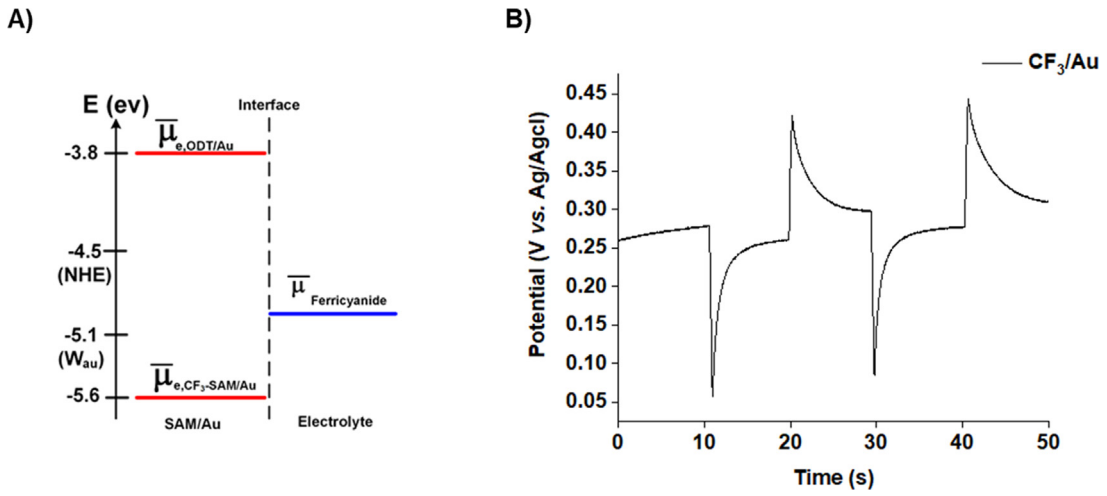

Fig. 3. (A) Energy diagram for the Au electrode according to kind of SAMs. (B) Potential responses to the 5000 μm lift/immersion of the CF_3/Au electrode from/in the solution of 1 mM $Fe(CN)_6^{3-}$ with 0.1 M KCl.

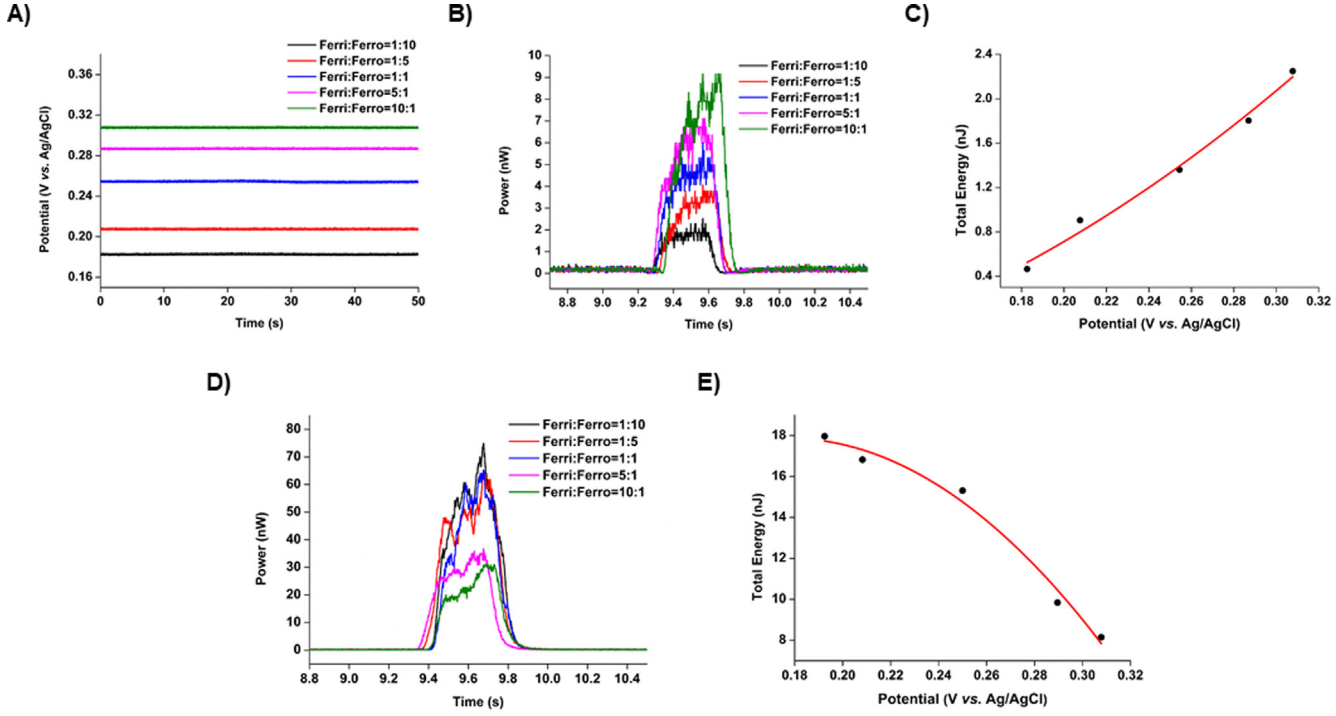

Fig. 4. (A) Measured $\bar{\mu}_{solution}$ from the open-circuit potential (OCP) depending on the ratio of the redox couple of $Fe(CN)_6^{3-}$/$Fe(CN)_6^{4-}$, where the total concentration was held at 5 mM. (B) Generated power through a 20 kΩ resistor at 5000 μm of displacement of the ODT/Au electrode at a speed of 13 mm/s, corresponding to different compositions of the electrolyte. (C) Estimated relationship between the total generated energy of ODT/Au and the electrochemical potential of the solution. (D) Power produced with the use of the CF_3/Au electrode under experimental conditions identical to those of ODT/Au. (E) Quadratic relationship between the total generated energy of CF_3/Au and the potential following energy of a capacitor.

CF_3 SAM induce a partial positive charge due to the high electronegativity of fluorine at the ω position as shown in Fig. 3A. Compared to the increased potential upon the lift shown in Fig. 1C for the ODT SAM, the voltage of CF_3/Au decreases upon the same motion, as shown in Fig. 3B. The excess charge on the metal is positive for ODT while it is negative for CF_3 as a result of the reverse surface dipole. As shown in Fig. 1A and Fig. 3B, the voltage change when lifting CF_3/Au (218.3 mV) is approximately two times larger than that of ODT/Au (105.4 mV), despite the fact that the difference in the work function between the CF_3/Au and the electrolyte is smaller. We speculate that the deviation of the work function due to the changing environment from the vacuum to the electrolyte or the smaller dielectric constant of the CF_3 SAM may cause this rise in the voltage [25]. Additionally, the dipole of the SAM and the intrinsic work function of the conducting phase are crucial for electrification at the solid-liquid interface [31,32]. Recently, the dipole of a SAM was found to be tunable by an external voltage, resulting in a different organic reaction called the electro-inductive effect [34]. Our results demonstrate the reverse process of the potential tuned by the internal dipole of molecules.

The electrochemical potential of the solution ($\bar{\mu}_{solution}$) is another significant parameter which drives the electrification according to

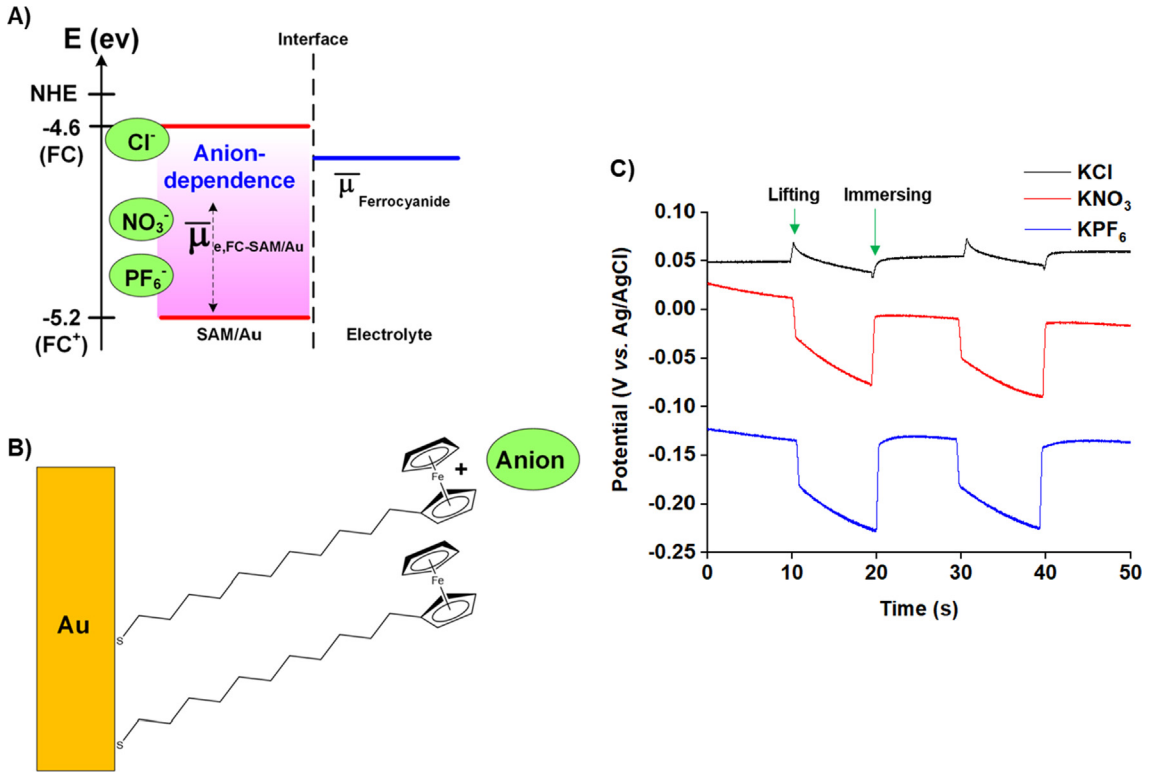

Fig. 5. (A) Energy diagram for the work functions tuned by the oxidation state of Fc and anion species in the electrolyte. (B) Schematic illustration for the interaction between Fc and anions. (C) Potential responses to the 5000 μm lift/immersion of the Fc/Au electrode from/in the electrolyte of 1 mM $Fe(CN)_6^{4-}$ with 0.1 M K^+X^- (X^-: PF_6^-, NO_3^-, and Cl^-).

the potential difference between $\bar{\mu}_{e,Au}$ and $\bar{\mu}_{solution}$. $\bar{\mu}_{solution}$ depends on the chemical composition in the presence of redox couple such as $Fe(CN)_6^{3-}/Fe(CN)_6^{4-}$ from the Nernst equation:

$$\bar{\mu}_{solution} = E^0_{Fe(CN)_6^{3-}/Fe(CN)_6^{4-}} - \frac{RT}{F}\ln\frac{a_{Fe(CN)_6^{4-}}}{a_{Fe(CN)_6^{3-}}} \quad (1)$$

Here, E^0 is the standard reduction potential of the redox couple, R is the gas constant, F is the Faraday constant, T is the temperature, and a_x denotes the activity of the chemical species *x*. Fig. 4A shows the open-circuit potential of the SAM/Au depending on the ratio of $Fe(CN)_6^{3-}/Fe(CN)_6^{4-}$, which follows eq. (1). When $\bar{\mu}_{e,Au}$ of ODT/Au is fixed at −3.8 eV (ca. −0.85 V *vs.* Ag/AgCl), the potential difference across the interface would be on the order of 1:10, 1:5, 1:1, 5:1 and 10:1 ($Fe(CN)_6^{3-}/Fe(CN)_6^{4-}$). With variations of the chemical composition, the power generated from the mechanical displacement of the ODT/Au electrode at a speed of 13 mm/s is illustrated in Fig. 4B. As can be observed, the larger $\bar{\mu}_{solution}$ is, the more power is produced due to the larger potential difference with $\bar{\mu}_{e,Au}$ according to the mechanism proposed here. In Fig. 4C, the total generated energy was determined by integration, demonstrating a quadratic relationship with potential following the energy of the capacitor, $E = (C \cdot V^2)/2$. For the CF_3/Au case, $\bar{\mu}_{e,Au}$ is much higher, at −5.6 eV (ca. 0.88 V *vs.* Ag/AgCl). Thus, both the polarity and quantity of electrification reveals an opposite trend compared to those of ODT/Au, as shown in Fig. 4D. Regarding the total generated energy, a clear quadratic relationship is also estimated, as illustrated in Fig. 4E, while the values of the energy are tens of nJ under this experimental condition. It should be noted that the contact angles of both ODT/Au and CF_3/Au show the similar values of ca. 110°, indicating the similar surface free energies of each other, which are consistent with previous reports [35–38] (Fig. S3 in the Supplementary Information). Thus, it can be concluded that the hydrophobicity or surface free energy does not affect the degree of electrification. Therefore, the validity of the suggested mechanism for electrification in our system is further supported.

The proposed mechanism was investigated further by examining the redox properties of an 11-(ferrocenyl)undecanethiol SAM. A ferrocene (Fc) group at the ω-position renders the electrode surface hydrophobic, similar to both ODT and CF_3 SAMs [39]. The work function, however, varies with the oxidation state of Fc, ranging from 4.6 eV for the fully reduced form (Fc) to 5.2 eV for the fully oxidized form (Fc^+) [40]. The standard reduction potential (E^0) of the Fc SAM strongly depends on the nature of the anions because Fc^+ favors strong interaction with hydrophobic counter ions, as shown in Fig. 5B [41], resulting in a lower E^0 for more hydrophobic anions. Thus, the energy level (i.e., the oxidation state) of the Fc/Au electrode varies with the nature of the anions (Fig. S4, Supplementary Information). When Fc/Au comes into contact with a solution containing $Fe(CN)_6^{4-}$ with 0.1 M K^+X^- (X^-: PF_6^-, NO_3^-, and Cl^-) electrolytes, some part of the Fc is oxidized in the presence of hydrophobic PF_6^- ions, whereas Fc retains its reduced state in hydrophilic Cl^- ions, as shown in Fig. 5A. In turn, the work function of Fc/Au is finely adjusted by the interface dipoles, which would be charged positively with Cl^- ions and negatively with both NO_3^- and PF_6^- ions. Fig. 5C presents the dependence of the potential on the anion species in the periodic motion of the SAM-modified electrodes in the electrolyte. In the solution containing Cl^- ions, the potential change (black line) indicates behavior opposite to those in the NO_3^- and PF_6^- cases. Moreover, it should be noted that anions do not adsorb onto the surface in the absence of the oxidation of Fc, in contrast to the previously proposed electrification of a solid-liquid interface [42]. Overall, from the experiments, the electrification of the solid-liquid interface is proved to be governed by (1) the work function of the solid electrode by dipoles dependent on either permanent polarity (ODT and CF_3) or the redox-active polarity

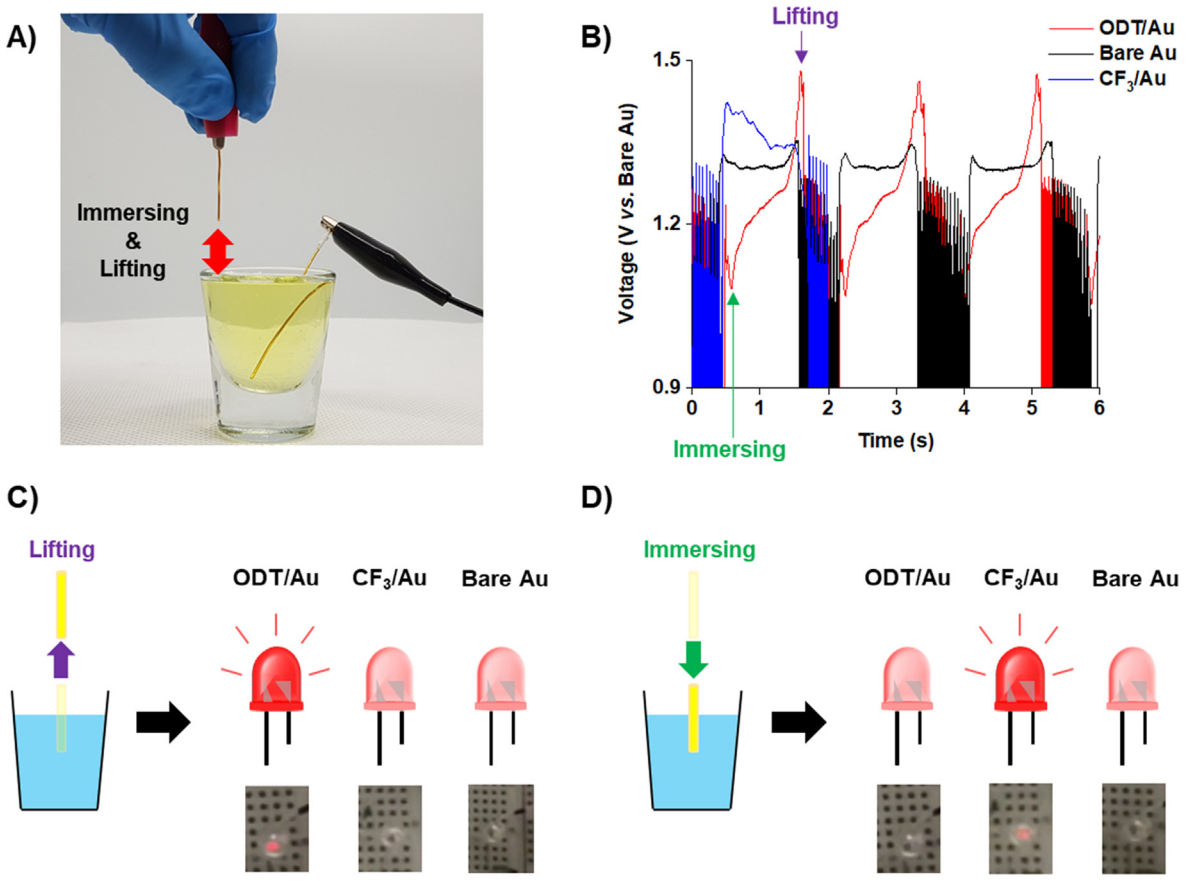

Fig. 6. Energy harvester based on the electrification between the SAM/Au wire and electrolyte. (A) Experimental set-up for a hybrid cell where a SAM/Au and a counter Au are connected to red clip (+) and black clip (−) of DAQ, respectively and used in the electrolyte of 1 mM $Fe(CN)_6^{3-}$ with 0.1 M KCl. (B) Potential responses to the immersing/lifting motions of the ODT/Au (red), CF_3/Au (blue) and bare Au (black) wires in/from the electrolyte. Captured and schematic images of the on-off LED by (C) lifting or (D) immersing ODT/Au, CF_3/Au, and bare Au electrodes.

states of SAMs, (2) the electrochemical potential of the electrolyte according to the corresponding composition, (3) the capacitance and resistance of the SAMs, and (4) the surface energy.

For a more in-depth assessment of our simple system, the generation and delivery of electrical energy were investigated by turning a LED on and off. To drive the LED, a hybrid power source with a serial connection consisting of a 1.2 V Ni-MH battery and our electrochemical cell was adopted. It should be noted that a Ni-MH battery cannot solely drive a LED. Fig. 6A illustrates an electrochemical cell composed of a SAM/Au (red clip) and bare Au (black clip) electrodes, with the former being immersed/lifted manually while the latter remained fixed. The red line in Fig. 6B represents the voltage of this hybrid power source upon mechanical motion, whose average value is around 1.2 V, close to that of a Ni-MH battery. As for the ODT/Au wire, immersion into the electrolyte increases the contact area, resulting in a decrease in the voltage, consistent with the first experiment, while lifting motion generates positive voltage in addition to the battery which turned the LED on, as shown in Fig. 6C (see Movie S1-S2 in the Supplementary Material). The polarity of the energy harvester is reversed as expected when using a CF_3/Au electrode (blue line in Fig. 6B) as explained earlier. Therefore, the LED was turned on during the immersing motion instead of lifting motion in the ODT/Au case (Fig. 6D). As a control experiment, applying mechanical motion to a bare Au wire (black line in Fig. 6B) indicates no voltage change. In general, this simple experiment has proven the mechanism of charging at the triple-phase boundary and the feasible implementation of an energy harvester based on water motions. In fact, the obtained power is only tens of nW at a translation speed of 13 mm/s with a 1-cm-wide electrode. Even though the mechanism is mainly investigated in our paper, a comparison of our simple model system with previous reports on harvesting energy from water may offer the insight. It should be mentioned that there is no standard figure-of-merits such as efficiency of output energy over mechanical energy, standard mechanical perturbation, surface area, and so on, which makes direct comparison without normalization unfair. From Table S1 (Supplementary Information), the generated power of our SAM/Au electrodes with adjustable electrochemical potential of solution shows the similar order of magnitude compared to those of studies based on carbon materials and polymer-coated system. Although the improvement in the power and efficiency is out of the scope at this stage, it can be expected in future explorations according to the operation mechanism. For more efficient energy harvester, it is suggested that: (1) the functional coating on the solid electrode should be (a) more hydrophobic to minimize the wetting of water, (b) sufficiently impeditive to charge transfer across solid/liquid interface, (c) more polar in normal direction to electrode surface, and (d) larger in dielectric constant; (2) the electrochemical potential of liquid solution should have the larger difference from that of electrode. There are also several types of mechanical perturbation, including periodic wave, dropping of water, and water evaporation, which may need further optimization in the configuration. Thus, our finding shows the ways to design and improve the energy harvesting of water movement.

4. Conclusions

The dependence of electrode potential on the contact area with electrolyte was investigated using the simple model system of the SAM/Au. The electrode potential of the SAM/Au at the triple-phase boundary of solid/liquid/air shows the unprecedented offset from the steady-state voltage. The interface between solid and liquid was charged by the difference of the electrochemical potential or work function, followed by the change in charge density during the mechanical motion. In the experiments, the SAM on the electrode surface is the key, offering (1) hydrophobicity, (2) a barrier for the charge transfer across the EDL, (3) a dipole to tune $\bar{\mu}_{e,Au}$, and (4) dielectric material for the capacitance. These results demonstrate that the electrification at the solid/liquid interface is driven by the difference in energy, which can be achieved by tuning either $\bar{\mu}_{solution}$ and $\bar{\mu}_{e,Au}$. The hybrid system also shows the possibility of our system to harvest the energy from electrolyte motions.

CRediT authorship contribution statement

Changsuk Yun: Investigation, Resources, Data curation, Writing – review & editing. **Thanh Duc Dinh:** Investigation, Data curation, Validation, Formal analysis, Writing – review & editing. **Seongpil Hwang:** Conceptualization, Methodology, Writing – original draft, Supervision, Funding acquisition.

Declaration of Competing Interest

The authors declare that they have no known competing financial interests or personal relationships that could have appeared to influence the work reported in this paper.

Acknowledgements

S.H. acknowledges the support from Basic Science Research Program through the National Research Foundation of Korea (NRF) grant funded by the Korea Government (MSIP) (No. NRF-2019R1A2C1089951).

Appendix A. Supplementary material

Supplementary data to this article can be found online at https://doi.org/10.1016/j.jcis.2022.01.114.

References

[1] L.R. Faulkner, A.J. Bard, E. Methods, Fundamentals and Applications, second ed., John Wiley & Sons, New York, 2001.
[2] I.L. Geada, H. Ramezani-Dakhel, T. Jamil, M. Sulpizi, H. Heinz, Insight into induced charges at metal surfaces and biointerfaces using a polarizable Lennard-Jones potential, Nat. Commun. 9 (1) (2018) 716.
[3] A.P. Willard, S.K. Reed, P.A. Madden, D. Chandler, Water at an electrochemical interface—a simulation study, Faraday Discuss. 141 (2009) 423–441.
[4] D.C. Grahame, The Electrical Double Layer and the Theory of Electrocapillarity, Chem. Rev. 41 (3) (1947) 441–501.
[5] G. Xue, Y. Xu, T. Ding, J. Li, J. Yin, W. Fei, Y. Cao, J. Yu, L. Yuan, L. Gong, J. Chen, S. Deng, J. Zhou, W. Guo, Water-evaporation-induced electricity with nanostructured carbon materials, Nat. Nanotechnol. 12 (4) (2017) 317–321.
[6] J. Tan, J. Duan, Y. Zhao, B. He, Q. Tang, Generators to harvest ocean wave energy through electrokinetic principle, Nano Energy 48 (2018) 128–133.
[7] R. Schweiss, P.B. Welzel, C. Werner, W. Knoll, Interfacial charge of organic thin films characterized by streaming potential and streaming current measurements, Colloids Surf. A 195 (1) (2001) 97–102.
[8] M. Safaei, H.A. Sodano, S.R. Anton, A review of energy harvesting using piezoelectric materials: state-of-the-art a decade later (2008–2018), Smart Mater. Struct. 28 (11) (2019) 113001.
[9] C. Wu, A.C. Wang, W. Ding, H. Guo, Z.L. Wang, Triboelectric Nanogenerator: A Foundation of the Energy for the New Era, Adv. Energy Mater. 9 (1) (2019) 1802906.
[10] W. Xu, H. Zheng, Y. Liu, X. Zhou, C. Zhang, Y. Song, X. Deng, M. Leung, Z. Yang, R. X. Xu, Z.L. Wang, X.C. Zeng, Z. Wang, A droplet-based electricity generator with high instantaneous power density, Nature 578 (7795) (2020) 392–396.
[11] S.H. Kim, C.S. Haines, N. Li, K.J. Kim, T.J. Mun, C. Choi, J. Di, Y.J. Oh, J.P. Oviedo, J. Bykova, S. Fang, N. Jiang, Z. Liu, R. Wang, P. Kumar, R. Qiao, S. Priya, K. Cho, M. Kim, M.S. Lucas, L.F. Drummy, B. Maruyama, D.Y. Lee, X. Lepró, E. Gao, D. Albarq, R. Ovalle-Robles, S.J. Kim, R.H. Baughman, Harvesting electrical energy from carbon nanotube yarn twist, Science 357 (6353) (2017) 773–778.
[12] J. Yin, Z. Zhang, X. Li, J. Yu, J. Zhou, Y. Chen, W. Guo, Waving potential in graphene, Nat. Commun. 5 (1) (2014) 3582.
[13] A.G. Banpurkar, Y. Sawane, S.M. Wadhai, C.U. Murade, I. Siretanu, D. van den Ende, F. Mugele, Spontaneous electrification of fluoropolymer–water interfaces probed by electrowetting, Faraday Discuss. 199 (2017) 29–47.
[14] C.-H. Lin, G.S. Ferguson, M.K. Chaudhury, Electrokinetics of Polar Liquids in Contact with Nonpolar Surfaces, Langmuir 29 (25) (2013) 7793–7801.
[15] J. Nie, Z. Ren, L. Xu, S. Lin, F. Zhan, X. Chen, Z.L. Wang, Probing Contact-Electrification-Induced Electron and Ion Transfers at a Liquid-Solid Interface, Adv. Mater. 32 (2) (2020) 1905696.
[16] G. Liu, T. Chen, J. Xu, G. Li, K. Wang, Solar evaporation for simultaneous steam and power generation, J. Mater. Chem. A 8 (2) (2020) 513–531.
[17] G. Liu, T. Chen, J. Xu, K. Wang, Blue energy harvesting on nanostructured carbon materials, J. Mater. Chem. A 6 (38) (2018) 18357–18377.
[18] Z. Zhang, X. Li, J. Yin, Y. Xu, W. Fei, M. Xue, Q. Wang, J. Zhou, W. Guo, Emerging hydrovoltaic technology, Nat. Nanotechnol. 13 (12) (2018) 1109–1119.
[19] L.S. McCarty, G.M. Whitesides, Electrostatic Charging Due to Separation of Ions at Interfaces: Contact Electrification of Ionic Electrets, Angew. Chem. Int. Ed. 47 (12) (2008) 2188–2207.
[20] S. Lin, M. Zheng, J. Luo, Z.L. Wang, Effects of Surface Functional Groups on Electron Transfer at Liquid-Solid Interfacial Contact Electrification, ACS Nano 14 (8) (2020) 10733–10741.
[21] S. Lin, X. Chen, Z.L. Wang, The tribovoltaic effect and electron transfer at a liquid-semiconductor interface, Nano Energy 76 (2020) 105070.
[22] P. Ma, H. Zhu, H. Lu, Y. Zeng, N. Zheng, Z.L. Wang, X. Cao, Design of biodegradable wheat-straw based triboelectric nanogenerator as self-powered sensor for wind detection, Nano Energy 86 (2021) 106032.
[23] S. Lin, X. Chen, Z.L. Wang, Contact Electrification at the Liquid-Solid Interface, Chem. Rev. (2021), https://doi.org/10.1021/acs.chemrev.1c00176.
[24] S. Lin, L. Xu, A. Chi Wang, Z.L. Wang, Quantifying electron-transfer in liquid-solid contact electrification and the formation of electric double-layer, Nat. Commun. 11 (1) (2020) 399.
[25] B. de Boer, A. Hadipour, M.M. Mandoc, T. van Woudenbergh, P.W.M. Blom, Tuning of Metal Work Functions with Self-Assembled Monolayers, Adv. Mater. 17 (5) (2005) 621–625.
[26] J.F. Smalley, Potential of Zero Charge and Its Temperature Derivative for Au (111) Electrode|Alkanethiol SAM|1.0 M Aqueous Electrolyte Solution Interfaces: Impact of Electrolyte Solution Ionic Strength and Its Effect on the Structure of the Modified Electrode|Electrolyte Solution Interface, J. Phys. Chem. C 121 (17) (2017) 9260–9272.
[27] D.M. Alloway, M. Hofmann, D.L. Smith, N.E. Gruhn, A.L. Graham, R. Colorado, V. H. Wysocki, T.R. Lee, P.A. Lee, N.R. Armstrong, Interface Dipoles Arising from Self-Assembled Monolayers on Gold: UV−Photoemission Studies of Alkanethiols and Partially Fluorinated Alkanethiols, J. Phys. Chem. B 107 (42) (2003) 11690–11699.
[28] J. Yang, J. Han, K. Isaacson, D.Y. Kwok, Effects of Surface Defects, Polycrystallinity, and Nanostructure of Self-Assembled Monolayers for Octadecanethiol Adsorbed onto Au on Wetting and Its Surface Energetic Interpretation, Langmuir 19 (22) (2003) 9231–9238.
[29] M. Jalal Uddin, M. Khalid Hossain, M.I. Hossain, W. Qarony, S. Tayyaba, M.N.H. Mia, M.F. Pervez, S. Hossen, Modeling of self-assembled monolayers (SAMs) of Octadecanethiol and Hexadecanethiol on gold (Au) and silver (Ag), Res. Phys. 7 (2017) 2289–2295.
[30] W.-G. Kim, D.-W. Kim, I.-W. Tcho, J.-K. Kim, M.-S. Kim, Y.-K. Choi, Triboelectric Nanogenerator: Structure, Mechanism, and Applications, ACS Nano 15 (1) (2021) 258–287.
[31] N.T. Plymale, A.A. Ramachandran, A. Lim, B.S. Brunschwig, N.S. Lewis, Control of the Band-Edge Positions of Crystalline Si(111) by Surface Functionalization with 3,4,5-Trifluorophenylacetylenyl Moieties, J. Phys. Chem. C 120 (26) (2016) 14157–14169.
[32] Q. Chen, C. Wang, Y. Li, L. Chen, Interfacial Dipole in Organic and Perovskite Solar Cells, J. Am. Chem. Soc. 142 (43) (2020) 18281–18292.
[33] T.G. Morrissey, S.K. Mitchell, A.T. Jaros, E. Ambos, C. Keplinger, Mechanical-to-Electrical Energy Conversion with Variable Electric Double Layers, Energy Technol. 7 (4) (2019) 1801007.
[34] J. Heo, H. Ahn, J. Won, J.G. Son, H.K. Shon, T.G. Lee, S.W. Han, M.-H. Baik, Electro-inductive effect: Electrodes as functional groups with tunable electronic properties, Science 370 (6513) (2020) 214–219.
[35] P.E. Laibinis, G.M. Whitesides, D.L. Allara, Y.T. Tao, A.N. Parikh, R.G. Nuzzo, Comparison of the structures and wetting properties of self-assembled monolayers of n-alkanethiols on the coinage metal surfaces, copper, silver, and gold, J. Am. Chem. Soc. 113 (19) (1991) 7152–7167.
[36] H. Notsu, W. Kubo, I. Shitanda, T. Tatsuma, Super-hydrophobic/super-hydrophilic patterning of gold surfaces by photocatalytic lithography, J. Mater. Chem. 15 (15) (2005) 1523–1527.
[37] A. Amirfazli, D.Y. Kwok, J. Gaydos, A.W. Neumann, Line Tension Measurements through Drop Size Dependence of Contact Angle, J. Colloid Interface Sci. 205 (1) (1998) 1–11.

[38] M. Graupe, M. Takenaga, T. Koini, R. Colorado, T.R. Lee, Oriented Surface Dipoles Strongly Influence Interfacial Wettabilities, J. Am. Chem. Soc. 121 (13) (1999) 3222–3223.
[39] J. Kim Yun, J. Kim Ki, Y. Jung Seung, J. Hwang You, J. Kwon Seong, Redox-Active Self-Assembled Monolayer on Au ultramicroelectrode and its Electrocatalytic Detection of p-aminophenol Oxidation, J. Electrochem Sci. Technol. 10 (2) (2019) 170–176.
[40] R.A. Wong, Y. Yokota, M. Wakisaka, J. Inukai, Y. Kim, Discerning the Redox-Dependent Electronic and Interfacial Structures in Electroactive Self-Assembled Monolayers, J. Am. Chem. Soc. 140 (42) (2018) 13672–13679.
[41] G. Valincius, G. Niaura, B. Kazakevičienė, Z. Talaikytė, M. Kažemėkaitė, E. Butkus, V. Razumas, Anion Effect on Mediated Electron Transfer through Ferrocene-Terminated Self-Assembled Monolayers, Langmuir 20 (16) (2004) 6631–6638.
[42] W. Fei, C. Shen, S. Zhang, H. Chen, L. Li, W. Guo, Waving potential at volt level by a pair of graphene sheets, Nano Energy 60 (2019) 656–660.